J|A|C|S ARTICLES

Published on Web 01/28/2009

$Gd_5Si_{4-x}P_x$: Targeted Structural Changes through Increase in Valence Electron Count

Volodymyr Svitlyk,[†] Gordon J. Miller,[‡] and Yurij Mozharivskyj*,[†]

Department of Chemistry, McMaster University, Hamilton, Ontario, L8S 4M1, Canada, and Department of Chemistry, Iowa State University, Ames, Iowa 50011

Received October 29, 2008; E-mail: mozhar@mcmaster.ca

Abstract: Phase transformations in the $Gd_5Si_{4-x}P_x$ system ($0 \leq x \leq 2$), studied through X-ray diffraction techniques, reveal an intimate coupling between the crystal structure and valence electron count. An increase in the valence electron count through P substitution results in breaking the interslab $T-T$ dimers ($d_{T-T} = 3.74$ Å; T is a mixture of Si and P) and shear movement of the $_\infty^2[Gd_5T_4]$ slabs in $Gd_5Si_{2.75}P_{1.25}$. The $Gd_5Si_{2.75}P_{1.25}$ phase extends the existence of the orthorhombic Sm_5Ge_4-type structures to the valence electron count larger than 31 e^-/formula unit. Tight-binding linear-muffin-tin-orbital calculations trace the origin of the $T-T$ dimer cleavage in $Gd_5Si_{2.75}P_{1.25}$ to a larger population of antibonding states within the dimers.

Introduction

Discovery of the giant magnetocaloric effect in $Gd_5Si_2Ge_2$,[1] followed by a successful test of a rotary magnetic refrigerator,[2,3] showed that the magnetocaloric effect may be beneficially utilized for room-temperature refrigeration and air conditioning. The unique feature which makes $Gd_5Si_2Ge_2$ and other materials, like $MnFeP_{1-x}As_x$, suitable for practical applications is an intrinsic coupling between a first-order structural transition and ferromagnetic ordering.[4,5] As a result, the entropy change is significantly increased (nearly doubled in $Gd_5Si_2Ge_2$ for $\Delta H = 0-5$ T) and the magneto-structural transformation yields a large temperature response to magnetic field.[6] The origin of structural transformations in $Gd_5Si_2Ge_2$ and related phases can be traced back to the interslab $T-T$ dimer cleavage and formation (T is a mixture of main group elements, viz., Si, Ge, Sn, and Ga) and, associated with that, movement of the $_\infty^2[Gd_5T_4]$ slabs,[7] which are the main building blocks of these structures. Thus, the ability to control the $T-T$ bonds is a possibility to tune structural and physical properties of existing magnetocaloric materials and a route to design new phases.

The RE_5T_4 phases (RE is a rare-earth metal), except for some Si-rich La−Nd phases, adopt three related structures types: (1) the orthorhombic Gd_5Si_4-type with all interslab $T-T$ dimers intact (d_{T-T} = ca. 2.5 Å); (2) the monoclinic $Gd_5Si_2Ge_2$-type, in which the $T-T$ dimers between alternate layers are broken (d_{T-T} = ca. 3.4 Å); and (3) the orthorhombic Sm_5Ge_4-type with all interslab dimers broken.[4,8−16] The interslab dimers arise from one crystallographic site, called the $T1$ site. There are two additional sites for main group atoms, $T2$ and $T3$, which also form dimers, but these dimers reside inside the $_\infty^2[Gd_5T_4]$ slabs and are not perturbed during any structural transition.[7] As discussed later in the text and previously for some RE_5T_4 phases,[17−19] the chemical formulas of the three structure types can be written as $(RE^{3+})_5(T_2^{6-})_2(3e^-)$, $(RE^{3+})_5(T_2^{6-})_{1.5}(T^{4-})(2e^-)$ and $(RE^{3+})_5(T_2^{6-})(T^{4-})_2(e^-)$. The conduction electrons noted in these formulas reside in the region of the conduction band that consists of bonding $RE-RE$ and $RE-T$ states, but antibonding $T-T$ states. The suggested electron counting scheme for the

[†] McMaster University.
[‡] Iowa State University.

(1) Pecharsky, V. K.; Gschneidner, K. A., Jr. *Phys. Rev. Lett.* **1997**, *78*, 4494–4497.
(2) Zimm, C. B.; Sternberg, A.; Jastrab, A. G.; Boeder, A. M.; Lawton, L. M., Jr.; Chell, J. J. Rotating bed magnetic refrigeration apparatus. US patent 6526759, 2003.
(3) Zimm, C.; Boeder, A.; Chell, J.; Sternberg, A.; Fujita, A.; Fujieda, S.; Fukamichi, K. *Inter. J. Refrig.* **2006**, *29*, 1302–1306.
(4) Pecharsky, V. K.; Gschneidner, K. A., Jr. *J. Alloys Compd.* **1997**, *260*, 98–106.
(5) Tegus, O.; Brick, E.; Buschow, K. H. J.; de Boer, F. R. *Nature* **2002**, *415*, 150–152.
(6) Pecharsky, V. K.; Gschneidner, K. A., Jr. *Springer Ser. Mater. Sci.* **2005**, *79*, 199–222.
(7) Choe, W.; Pecharsky, V. K.; Pecharsky, A. O.; Gschneidner, K. A., Jr.; Young, V. G., Jr.; Miller, G. J. *Phys. Rev. Lett.* **2000**, *84*, 4617–4620.
(8) Gschneidner, K. A., Jr.; Pecharsky, V. K.; Pecharsky, A. O.; Ivtchenko, V. V.; Levin, E. M. *J. Alloys Compd.* **2000**, *303−304*, 214–222.
(9) Huang, H.; Pecharsky, A. O.; Pecharsky, V. K.; Gschneidner, K. A., Jr. *Adv. Cryog. Eng.* **2002**, *48*, 11–18.
(10) Pecharsky, V. K.; Pecharsky, A. O.; Gschneidner, K. A., Jr. *J. Alloys Compd.* **2002**, *344*, 362–368.
(11) Spichkin, Y. I.; Pecharsky, V. K.; Gschneidner, K. A., Jr. *J. Appl. Phys.* **2001**, *89*, 1738–1745.
(12) Pecharsky, V. K.; Pecharsky, A. O.; Mozharivskyj, Y.; Gschneidner, K. A., Jr.; Miller, G. J. *Phys. Rev. Lett.* **2003**, *91*, 207205/207201–204.
(13) Ahn, K.; Tsokol, A. O.; Mozharivskyj, Y.; Gschneidner, K. A., Jr.; Pecharsky, V. K. *Phys. Rev. B* **2005**, *72*, 054404/054401–11.
(14) Yang, H. F.; Rao, G. H.; Liu, G. Y.; Ouyang, Z. W.; Liu, W. F.; Feng, X. M.; Chu, W. G.; Liang, J. K. *Phys. B (Amsterdam)* **2003**, *325*, 293–299.
(15) Yang, H. F.; Rao, G. H.; Liu, G. Y.; Ouyang, Z. W.; Liu, W. F.; Feng, X. M.; Chu, W. G.; Liang, J. K. *J. Alloys Compd.* **2003**, *348*, 150–156.
(16) Yang, H. F.; Rao, G. H.; Liu, G. Y.; Ouyang, Z. W.; Liu, W. F.; Feng, X. M.; Chu, W. G.; Liang, J. K. *J. Alloys Compd.* **2002**, *346*, 190–196.
(17) Mozharivskyj, Y.; Choe, W.; Pecharsky, A. O.; Miller, G. J. *J. Am. Chem. Soc.* **2003**, *125*, 15183–15190.
(18) Mozharivskyj, Y.; Tsokol, A. O.; Miller, G. J. *Z. Kristallogr.* **2006**, *221*, 493–501.
(19) Wu, L.-M.; Kim, S.-H.; Seo, D.-K. *J. Am. Chem. Soc.* **2005**, *127*, 15682–15683.

Table 1. Crystallographic Data for the $Gd_5Si_{4-x}P_x$ Powders and Single Crystals

x	sample	str. type of phases	*a*, Å	*b*, Å	*c*, Å	*c/a*	*V*, Å^3
0	crystal	Gd_5Si_4	7.4743(5)	14.753(1)	7.7424(5)	1.0359(1)	853.7(1)
	powder	Gd_5Si_4	7.4827(4)	14.746(1)	7.7473(5)	1.0354(1)	854.9(1)
0.25	powder[a]	Gd_5Si_4	7.4910(5)	14.712(1)	7.7430(6)	1.0336(2)	853.3(1)
0.5	crystal	Gd_5Si_4[b] + Sm_5Ge_4	7.522(1)	14.698(3)	7.724(1)	1.0268(2)	853.9(3)
	powder	Gd_5Si_4[b]	7.4909(6)	14.692(1)	7.7504(6)	1.0346(1)	853.0(1)
		Sm_5Ge_4	7.5739(9)	14.671(2)	7.6686(9)	1.0125(2)	852.1(2)
0.75	crystal	Gd_5Si_4 + Sm_5Ge_4[b]	7.548(1)	14.661(3)	7.698(1)	1.0199(2)	851.9(3)
	powder	Gd_5Si_4	7.4916(9)	14.668(2)	7.7414(9)	1.0333(2)	850.7(2)
		Sm_5Ge_4[b]	7.5758(9)	14.664(2)	7.6653(8)	1.0118(2)	851.5(2)
1	crystal	Gd_5Si_4 + Sm_5Ge_4[b]	7.545(1)	14.669(2)	7.695(1)	1.0199(2)	851.7(3)
	powder	Gd_5Si_4	7.4890(8)	14.663(2)	7.751(1)	1.0350(4)	851.1(2)
		Sm_5Ge_4[b]	7.5834(8)	14.649(2)	7.6624(7)	1.0104(1)	851.2(1)
1.25	crystal	Sm_5Ge_4	7.607(2)	14.645(3)	7.684(2)	1.0101(4)	856.0(4)
	powder	Sm_5Ge_4	7.5913(7)	14.628(1)	7.6656(7)	1.0098(1)	851.2(1)
1.5	powder	Sm_5Ge_4	7.5935(5)	14.626(1)	7.6661(5)	1.0096(1)	851.4(1)
2	powder	Sm_5Ge_4	7.5946(5)	14.620(1)	7.6634(5)	1.0091(1)	850.9(1)

[a] Cell parameters of the Sm_5Ge_4-type phase could not be reliably refined. [b] Dominant phase.

RE_5T_4 phases implies that their structures and, consequently, their properties can be governed by the valence electron count (VEC). This hypothesis was substantiated when the Gd_5Ge_4 phase with VEC = 31 e$^-$ and broken interslab dimers could reform the $T1-T1$ dimers through partial substitution of Ge by the size-equivalent triel Ga in $Gd_5Ga_xGe_{4-x}$ ($x = 1-2$, VEC = 29−30 e$^-$).[17] Seo et al. subsequently demonstrated that lowering the VEC through substitution of trivalent La and Ce with divalent Ca also leads to $T1-T1$ dimer formation in $La_{5-x}Ca_xGe_4$ and $Ce_{5-x}Ca_xGe_4$.[19] So far, rigorous exploration of the relationship between VEC and structure for the RE_5X_4 phases has been limited to VEC ≤ 31 e$^-$ and focused on forming interslab dimers into the Sm_5Ge_4-type structures.

Alternatively, it should be possible to break interslab dimers in Gd_5Si_4-type structures with VEC = 31 e$^-$ by increasing the VEC. To explore structural responses of RE_5T_4 to higher VECs unambiguously, size-equivalent but electron-richer atoms must be introduced into a structure with interslab dimers intact. The $Gd_5Si_{4-x}P_x$ system was chosen for such studies because the parent Gd_5Si_4 phase contains interslab dimers, and similar atomic radii of Si and P (covalent radii, r_{cov}, of Si and P, respectively, are 1.17 and 1.10 Å)[20] will minimize possible matrix effects. In this paper, we report for the first time the synthesis and characterization of $Gd_5Si_{4-x}P_x$ phases, in which an increase in the VEC through P substitution was employed to break the Si−Si dimers of the parent Gd_5Si_4 phase. With this $Gd_5Si_{4-x}P_x$ series, we extend the existence of the RE_5T_4 phases adopting the Sm_5Ge_4-type structure into an electron-richer region, above the VEC of 31 e$^-$/formula unit, and have verified the prediction of breaking interslab dimers by replacing some Si atoms with P in Gd_5Si_4.

Experimental Section

Synthesis. According to our in-house analysis, the gadolinium powders purchased from several suppliers were severely contaminated with hydrogen. Since such light atom impurities may have a detrimental effect on physical and structural properties,[21,22] the synthesis of $Gd_5Si_{4-x}P_x$ phases had to proceed from bulk gadolinium. Starting materials included pieces of gadolinium (99.99 wt.%, distilled grade, Metall Rare Earth Limited, China), silicon (99.999 wt.%, Alfa Aesar), and phosphorus (99.999 wt.%, Puratronic, Alfa Aesar). To avoid introducing contaminants by filing gadolinium, pieces of Gd and Si in a 1:1 molar ratio were arc-melted to obtain the GdSi binary phase (FeB-type structure). The resulting GdSi product was ground in an Ar-filled glovebox and intimately mixed with ground phosphorus in the GdSi:P molar ratio of 1:1. This mixture was pressed, sealed in an evacuated silica tube, heated to 400 at 50 °C/hour, kept at this temperature for 12 h, then heated to 800 at 50 °C/hour, kept at this temperature for 48 h, and subsequently quenched in cold water. X-ray powder diffraction analysis indicated that P substituted for Si in GdSi to form the GdP binary phase (NaCl-type structure), thereby discharging elemental Si. This sample was then ground in the glovebox and pressed into seven tablets. Each tablet was combined with a proper amount of Gd and Si pieces to target $Gd_5Si_{4-x}P_x$ with compositions $x = 0.25$, 0.50, 0.75, 1.00, 1.25, 1.50, and 2.00, and the samples were arc-melted. During melting total losses were negligible, <0.2 wt.%. Any P losses, which would be recognized by a white deposit inside the chamber, could not be detected. Absence of any significant P losses can be explained by the fact that phosphorus was bound as an anion into the highly refractory GdP binary phase. The Gd_5Si_4 phase was prepared by directly arc-melting Gd and Si pieces; the resulting buttons were remelted at least 3 times to improve homogeneity.

X-Ray Analysis. Phase analyses and lattice constant refinements of the products were completed on a PANalytical X'Pert Pro diffractometer with a linear X'Celerator detector. Co$K\alpha$ radiation was used to avoid the Gd fluorescence associated with Cu$K\alpha$ radiation and to obtain a better resolution required for the refinement of the structurally similar and simultaneously present Gd_5Si_4- and Sm_5Ge_4-type phases. The unit cell parameters derived from a full-profile Rietveld refinement (*Rietica* program[23]) are summarized in Table 1. Amounts of the Gd_5Si_4- and Sm_5Ge_4-type phases were estimated using the same technique. The $Gd_5Si_{4-x}P_x$ samples with $x = 0.25-1.00$ were found to be mixtures of both Gd_5Si_4- and Sm_5Ge_4-type phases, with the amount of Sm_5Ge_4-type phase being proportional to the P concentration, x. Samples with $x = 1.25-2.00$ did not contain a Gd_5Si_4-type phase. However, at $x = 1.50$ and 2.00, large amounts of a GdP impurity were observed. Based on the phase analysis, it can be concluded that the Sm_5Ge_4-type phase of $Gd_5Si_{4-x}P_x$ appears in the region of $1.00 < x \leq 1.25$. The unit cell parameters, specifically a and c as well as the c/a ratio (Figure 1), point to some possible homogeneity for the Sm_5Ge_4-type phase. But this homogeneity is expected to be relatively small and unlikely to go much beyond $x = 1.25$, as the increase in the P content above $x = 1.25$ yields almost identical lattice constants and leads to a larger GdP presence.

(20) Pauling, L. C. *The Nature of the Chemical Bond and the Structure of Molecules and Crystals: An Introduction to Modern Structural Chemistry*, 3rd ed.; Cornell University Press: Ithaca, NY, 1960.
(21) Gschneidner, K. A., Jr.; Pecharsky, V. K. *J. Appl. Phys.* **1999**, *85*, 5365–5368.
(22) Mozharivskyj, Y.; Pecharsky, A. O.; Pecharsky, V. K.; Miller, G. J. *J. Am. Chem. Soc.* **2005**, *127*, 317–324.
(23) Hunter, B. A.; Howard, C. J. *Australian Nuclear Science and Technology Organization*: Menai: Austalia, 2000.

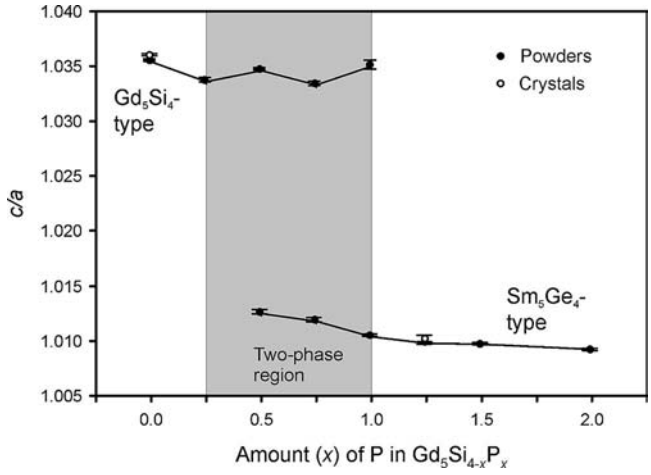

Figure 1. *c/a* ratio as a function of P amount. The gray area indicates a two-phase region as established from X-ray powder diffraction patterns at room temperature.

Single crystals were extracted from the samples with $x = 0$, 0.50, 0.75, 1.00 and 1.25. Room-temperature data were collected on a STOE IPDS II diffractometer with Mo Kα radiation. Numerical absorption corrections were based on the crystal shapes that were originally derived from optical face indexing, but later optimized against equivalent reflections using STOE *X-Shape* software.[24] Structural refinements were performed using the *SHELXL* program.[25] Significant crystallographic results are summarized in Tables 2 and 3. Since the atomic scattering factors of Si and P are nearly identical, the same Si/P statistical mixtures consistent with sample compositions were assumed on the three *T* sites. Nearest-neighbor bond distances could not be used to distinguish Si and P atoms adequately, because their similar atomic radii makes such analysis untenable.

Structural refinements for the crystals with $x = 0.50$, 0.75, and 1.00 produced positive residual electron density accompanying every atomic position. Additional crystals were tested for each sample, but identical results were obtained. The electron density maps generated from the experimental intensities showed a smeared, pear-shape electron density distribution around every atomic site. Comparison of these maps with those from Gd_5Si_4 and $Gd_5Si_{2.75}P_{1.25}$ (Figure 2) indicated that such electron density peaks result from the superposition of the two different structures, Gd_5Si_4 and $Gd_5Si_{2.75}P_{1.25}$. Presence of a possible superstructure, which could account for the diffuse electron density, was not supported due to the lack of additional Bragg reflections. Therefore, it was concluded that the crystals are twins of the Gd_5Si_4- and Sm_5Ge_4-type structures with similar unit cells but different atomic arrangements. Since the unit cell parameters of the Gd_5Si_4- and Sm_5Ge_4-type structures from the same $Gd_5Si_{4-x}P_x$ sample are quite similar (as judged from X-ray powder diffraction), peak splitting is small and could not be reliably detected due to the low spatial resolution of the area detector. Instead, the positions and intensities of the peaks originating from the two structures were averaged which resulted in the average unit cell dimensions and composite atomic arrangements during refinements. Indeed, the unit cell parameters of the crystals with $x = 0.50$, 0.75, and 1.00 fall between the values obtained for the Gd_5Si_4- and Sm_5Ge_4-type structures for the same sample. Annealing the samples with $x = 0.50$, 0.75, and 1.00 at 800 °C for two weeks did not eliminate the crystal twinning. Although unusual, such twinning has been previously observed in the two-phase regions of the $Gd_5Ga_xGe_{4-x}$ and $Gd_5Si_{4-x}Ge_x$ systems.[17,26] In $Gd_5Si_{1.5}Ge_{2.5}$, the composite nature of the crystals was traced to their microscopic inhomogeneity.[26] A similar compositional inhomogeneity can be assumed to exist on the microscopic level in the two-phase $Gd_5Si_{4-x}P_x$ samples. Further details of the crystal structure investigations can be obtained from the Fachinformationszentrum Karlsruhe, 76344 Eggenstein-Leopoldshafen, Germany, (fax: (49) 7247−808−666; e-mail: crysdata@fiz.karlsruhe.de) on quoting the depository CSD numbers 420010 for Gd_5Si_4 and 420011 for $Gd_5Si_{2.75}P_{1.25}$ and also from the Supporting Information.

Electronic Structure Calculations. Tight-binding, linear-muffin-tin-orbital calculations using the atomic sphere approximation (TB-LMTO-ASA)[27] were carried out for Gd_5Si_4 and a hypothetical "Gd_5Si_3P" with the Stuttgart program.[28] The lattice and atomic parameters from the $Gd_5Si_{2.75}P_{1.25}$ single crystal were used for the structure of "Gd_5Si_3P." Exchange and correlation were treated by the local density approximation (LDA).[29] All relativistic effects except spin−orbit coupling were taken into account by using a scalar relativistic approximation.[30] In the ASA method, space is filled with overlapping Wigner-Seitz (WS) atomic spheres, the radii of which were obtained by requiring the overlapping potential to be the best possible approximation to the full potential. This overlap should not be too large because the error in kinetic energy introduced by the combined correction is proportional to the fourth power of the relative sphere overlap. To satisfy the overlap criteria of the atomic spheres in the TB-LMTO-ASA method, empty spheres were included in the unit cell employing an automatic sphere generation.[31] The WS radii employed for these calculations are as follows: Gd = 1.75−1.81 Å, Si = 1.47−1.57 Å, *P* = 1.45−1.54 Å, and empty spheres = 0.69−1.06 Å. The basis sets included 6s, 6p, and 5d wave functions for Gd; 3s and 3p wave functions for Si and P; and 1s functions for the empty spheres. The Gd 6p orbitals were treated by the Löwdin downfolding technique,[27,29,30] and the 4f electrons of Gd were treated as core electrons. The *k*-space integrations were performed by the tetrahedron method.[32] The self-consistent charge density was obtained using 256 irreducible *k*-points in the Brillouin zone for the orthorhombic cells.

Three different structural models were considered for "Gd_5Si_3P." In the first model, the P atoms were placed on one-half of the *T*1 sites in a way that the nearest P neighbors are only Si1 atoms (*Pnma* symmetry was reduced to $P2_1ma$); in two other models, the P atoms were placed, respectively, on the *T*2 and *T*3 sites.

Results and Discussion

Structural Changes. The phase transition in the $Gd_5Si_{4-x}P_x$ series, which occurs between Gd_5Si_4 and $Gd_5Si_{2.75}P_{1.25}$, can be characterized as a Gd_5Si_4-to-Sm_5Ge_4 transformation. Gd_5Si_4 adopts its own structure type, while $Gd_5Si_{2.75}P_{1.25}$ crystallizes with the Sm_5Ge_4-type structure. The detailed description of the two structure types can be found elsewhere,[4,33,34] so only a brief summary of the most important structural features will be presented here. The Gd_5Si_4-type and Sm_5Ge_4-type structures of the $Gd_5Si_{4-x}P_x$ series are built from nearly identical 3^2434 nets

(24) *STOE & Cie GmbH*; Darmstadt: Germany, 2004.
(25) Sheldrick, G. M. *SHELXL97* and *SHELXS97*; University of Gottingen: Germany, 1997.
(26) Choe, W.; Miller, G. J.; Meyers, J.; Chumbley, S.; Pecharsky, A. O. *Chem. Mater.* **2003**, *15*, 1413–1419.
(27) Anderson, O. K. *Phys. Rev. B* **1986**, *34*, 2439.
(28) Jepsen O., Burkhardt A., Anderson O. K. *The TB-LMTO-ASA Program, version 4.7, Max-Planck-Institut für Festkörperforschung*; Stuttgart: Germany 1999.
(29) Anderson, O. K.; Jepsen, O. *Phys. Rev. Lett.* **1984**, *53*, 2571.
(30) >Anderson, O. K. Jepsen, O., Glötzel D. In *Highlights of condensed matter theory*; Bassani, F., Fumi, F., Tosi, M., Eds.; Lambrecht, W. R. L.: New York, 1985.
(31) Jepsen, O.; Anderson, O. K. *Z. Phys. B* **1995**, *97*, 35.
(32) Blöchl, P. E.; Jepsen, O.; Anderson, O. K. *Phys. Rev. B* **1994**, *49*, 16223.
(33) Le Roy, J.; Moreau, J. M.; Paccard, D.; Parthe, E. *Acta Crystallogr. B* **1978**, *B34*, 3315–3318.
(34) Holtzberg, F.; Gambino, R. J.; McGuire, T. R. *J. Phys. Chem. Solids* **1967**, *28*, 2283–2289.

Table 2. Crystal Data and Structure Refinements for Gd_5Si_4 and $Gd_5Si_{2.75}P_{1.25}$ at 293 K, Mo$K\alpha_1$ Radiation, STOE IPDS II Diffractometer

composition	Gd_5Si_4	$Gd_5Si_{2.75}P_{1.25}$
Space group	*Pnma*	*Pnma*
Lattice parameters (Å)	$a = 7.4743(5)$	$a = 7.607(2)$
	$b = 14.7529(7)$	$b = 14.645(3)$
	$c = 7.7424(4)$	$c = 7.684(2)$
Volume (Å^3)	853.74(8)	856.0(4)
Z	4	4
Density (calculated), g/cm^3	6.991	7.000
Crystal size, mm^3	$0.09 \times 0.11 \times 0.17$	$0.05 \times 0.07 \times 0.08$
2θ range for data collection	5.94 to 58.30°	5.76 to 56.56°
Index ranges	$-10 \le h \le 10$, $-20 \le k \le 16$, $-10 \le l \le 10$	$-10 \le h \le 9$, $-19 \le k \le 19$, $-6 \le l \le 10$
Reflections collected	8147	6432
Independent reflections	1192 [$R_{int} = 0.0712$]	1065 [$R_{int} = 0.0494$]
Completeness to max 2θ	99.8%	96.7%
Data/restraints/parameters	1192/0/47	1095/0/47
Goodness-of-fit on F^2	1.089	1.112
Final R indices [$I > 2\sigma(I)$]	$R_1 = 0.0344$, $wR_2 = 0.0749$	$R_1 = 0.0754$, $wR_2 = 0.1633$
R indices (all data)	$R_1 = 0.0419$, $wR_2 = 0.0774$	$R_1 = 0.0823$, $wR_2 = 0.1665$
Extinction coefficient	0.00356(19)	0.00063(11)
Largest diff. peak/ hole, e$^-$/Å^3	2.800/−2.802	5.769/−3.944

Table 3. Atomic and Isotropic Temperature (U_{eq}) Parameters for Gd_5Si_4 and $Gd_5Si_{2.75}P_{1.25}$ from Single Crystal Diffraction Data

atom	site	occupancy	*x/a*	*y/b*	*z/c*	U_{eq} (Å^2)
Gd_5Si_4						
Gd1	8*d*	1	0.02881(5)	0.59724(3)	0.18263(5)	0.0110(2)
Gd2	8*d*	1	0.31646(5)	0.12238(3)	0.17964(5)	0.0095(2)
Gd3	4*c*	1	0.14440(7)	0.25	0.51113(7)	0.0094(2)
Si1	8*d*	1	0.1439(3)	0.0400(2)	0.4723(3)	0.0116(4)
Si2	4*c*	1	0.0214(4)	0.25	0.0996(4)	0.0112(6)
Si3	4*c*	1	0.2590(4)	0.25	0.8753(5)	0.0106(6)
$Gd_5Si_{2.75}P_{1.25}$						
Gd1	8*d*	1	−0.0380(2)	0.60363(8)	0.1765(2)	0.0110(3)
Gd2	8*d*	1	0.3916(2)	0.11477(8)	0.1650(2)	0.0105(3)
Gd3	4*c*	1	0.2205(2)	0.25	0.5013(2)	0.0091(3)
Si/P1	8*d*	0.69/0.31[a]	0.2275(9)	0.0469(4)	0.4772(9)	0.011(1)
Si/P2	4*c*	0.69/0.31[a]	0.0998(14)	0.25	0.1114(12)	0.012(2)
Si/P3	4*c*	0.69/0.31[a]	0.3309(13)	0.25	0.8748(13)	0.010(2)

[a] Si/P occupancy was not refined.

of Gd atoms (Figure 3). Two such nets are stacked over one another along the *b* axis to form two-dimensional slabs with Gd3 atoms in pseudocubic and *T*2, *T*3 main group atoms in trigonal prismatic voids. Since the trigonal prisms in these slabs share a face, the separation between the *T*2 and *T*3 atoms is small enough to allow dimer formation. The Gd pseudocubes are capped top and bottom by the *T*1 atoms, and the empirical composition of the slabs is identical to the overall composition of the phase, Gd_5T_4. Whereas in Gd_5Si_4 the $_\infty^2[Gd_5T_4]$ slabs are interconnected via Si1−Si1 bonds ($d_{Si1-Si1} = 2.49$ Å), all *T*1-*T*1 interslab bonds are broken ($d_{T1-T1} = 3.74$ Å) in $Gd_5Si_{2.75}P_{1.25}$. This bond cleavage is accompanied by a shear movement of the slabs primarily along the *a*-direction and an increase in the corresponding lattice parameter of the Sm_5Ge_4-type phases. This type of phase transition can be monitored in $Gd_5Si_{4-x}P_x$ through the *c/a* ratio, as proposed by Choe et al.[26] for $Gd_5Si_{4-x}Ge_x$ and also successfully applied to other related phases.[17,19] For the $Gd_5Si_{4-x}P_x$ powders, the *c/a* ratio changes discontinuously, which indicates a first-order structural transformation (Figure 1). For the single crystal data, the increase in *c/a* is smoother, with intermediate *c/a* values in the two-phase region, which is due to their unusual structural behavior in this region, as discussed above.

The shear movement of the $_\infty^2[Gd_5T_4]$ slabs in $Gd_5Si_{4-x}P_x$ is expected to alter interslab interactions more significantly than the intraslab ones. Indeed, using *T*-*T* dimer distances as a perturbation parameter, it can be seen that the atomic arrangements are only slightly disturbed within the slabs ($d_{T2-T3} = 2.53$ Å in $Gd_5Si_{2.75}P_{1.25}$ vs $d_{Si2-Si3} = 2.48$ Å in Gd_5Si_4), while significantly disrupted between the slabs ($d_{T1-T1} = 3.74$ Å vs $d_{Si1-Si1} = 2.49$ Å) along the Gd_5Si_4-to-$Gd_5Si_{2.75}P_{1.25}$ transition. A more detailed analysis of the interatomic distances supports this argument and reveals that the intraslab Gd-*T* and Gd−Gd bonds remain almost unaltered, whereas the interslab Gd-*T*1 bonds become appreciably shorter and Gd−Gd contacts somewhat larger (Table 4), as also seen in $Gd_5Si_{4-x}Ge_x$.[35] Such variations in the interatomic distances highlight the two unique features of the Gd_5T_4 structures, and the RE_5T_4 ones in general, namely the rigidity of the $_\infty^2[Gd_5T_4]$ slabs and flexibility of the interslab bonds. Thus, the interslab dimers in $Gd_5Si_{2.75}P_{1.25}$ respond to the larger VEC by breaking *T*1-*T*1 bonds, thereby accommodating the additional conduction electrons in the valence shell of these Si or P monomers. In this way, $Gd_5Si_{2.75}P_{1.25}$ with the VEC of 32.25 e$^-$ is able to preserve the $_\infty^2[Gd_5T_4]$ layers, i.e., the essential building units of the RE_5T_4 structures, while optimizing the interslab interactions. To understand the relationship between the increased VEC and the dimer cleavage in $Gd_5Si_{2.75}P_{1.25}$, we will first consider the electronic structure of Gd_5Si_4.

Electronic Structure of Gd_5Si_4. Qualitatively, the electronic structure of many intermetallic compounds containing main group elements can be successfully analyzed within the framework of the Zintl−Klemm electron counting formalism.[36] According to this concept, the Si dimers of Gd_5Si_4 are isoelectronic with halogen dimers and carry a formal negative charge of 6 (Si_2^{6-} dimers). If ionic interactions between the Si_2^{6-} dimers and Gd^{3+} cations are implied, only 28 valence electrons are required to optimize interactions. In reality, the Gd−Si interactions are far from being ionic. Furthermore, short Gd−Gd distances indicate strong bonding between the neighboring Gd atoms. Still treating the Gd atoms as Gd^{3+}, the chemical formula can be written as $(Gd^{3+})_5(Si_2^{6-})_2(3e^-)$. The three valence electrons in excess of 28 e$^-$ will occupy a mixture of Si−Si σ_p* antibonding states as well as Gd−Gd and Gd−Si bonding states.

(35) Misra, S; Miller, G. J. *J. Solid State Chem.* **2006**, *179*, 2290–2297.
(36) Miller, G. J. In *Chemistry, Structure, and Bonding of Zintl Phases and Ions*; Kauzlarich, S. M., Ed.; VCH Publishers, Inc.: New York, 1996; pp 1−59.

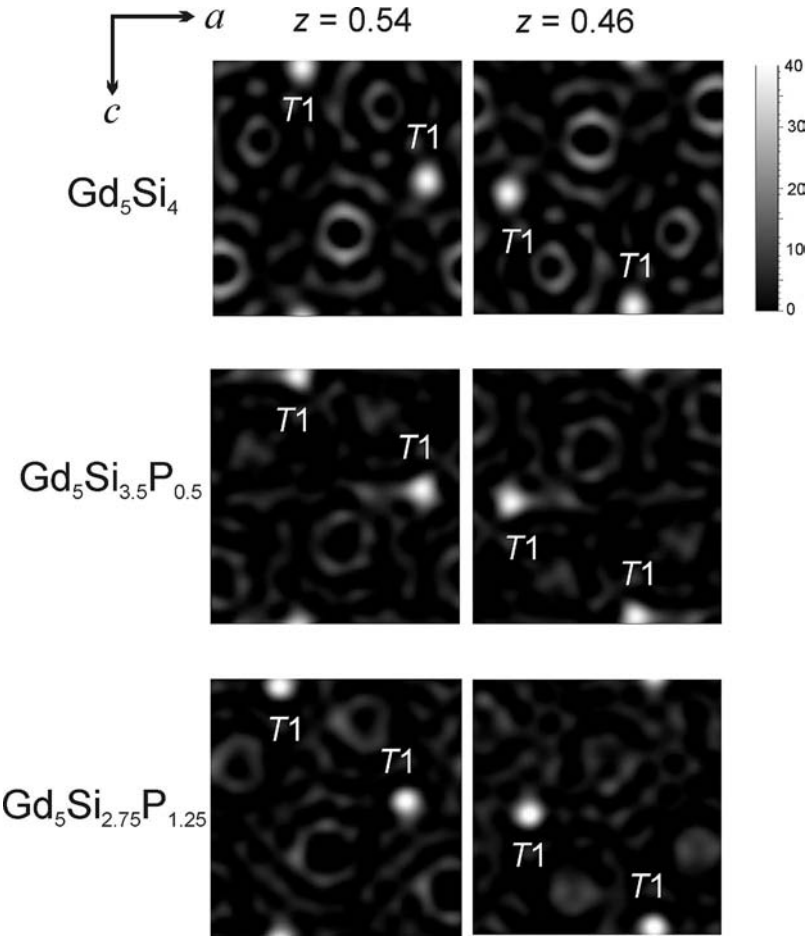

Figure 2. Electron density maps for Gd_5Si_4, $Gd_5Si_{3.5}P_{0.5}$ and $Gd_5Si_{2.75}P_{1.25}$. The planes from two different unit cells at two different z values are shown in order to emphasize changes in the $T1-T1$ dimer distances.

This simple bonding scheme is supported by TB-LMTO-ASA electronic structure calculations (Figures 4 and 5). In the density of states (DOS) and crystal orbital Hamilton population (COHP) plots, the two peaks around −8.5 and −6.5 eV represent, respectively, the bonding σ_s and antibonding σ_s* states from the Si_2 dimers, with some contribution from Gd orbitals. Due to the similar Si1−Si1 and Si2−Si3 bond lengths, the states originating from the two distinct dimers (Si1−Si1 and Si2−Si3) significantly overlap each other in the DOS curve. The valence band, which extends from −4.5 to −0.7 eV, is separated by a pseudogap from the conduction band. The states below −0.7 eV are derived primarily from the σ_p, π, and π* states of the Si_2 dimers mixed with Gd 6*s* and 5d orbitals. The states up to the pseudogap account for 28 valence electrons/formula, which agrees with the results obtained by the Zintl−Klemm approach. Presence of Gd states in this low-energy region is due to the interactions between the 3p lone pairs of the Si_2 dimers and Gd orbitals as well as to the Gd−Gd bonds.

The conduction band, which lies above −0.7 eV, has the largest contribution from Gd 5d and 6p orbitals and a small contribution from the σ_p* antibonding states within the Si_2 dimers. Analysis of the bonding characteristics by COHP curves indicates antibonding interslab and intraslab Si−Si interactions (Figure 5), with all other interactions being bonding around the Fermi level. The occupancy of the Si−Si σ_p* antibonding states indicates a potential electronic instability, which can be partially lifted by breaking interslab Si1−Si1 bonds as observed in Er_5Si_4 below 222 K.[37] However, in Gd_5Si_4, this instability is not observed to be lifted at low temperatures. Thus, other approaches, in particular variations in VEC, can be used to eliminate it.

Electronic Structure of "Gd_5Si_3P". Increasing the VEC through P substitution will have a destabilizing effect on both the intraslab and interslab $T-T$ dimers in the Gd_5Si_4-type phases. Thus, a structural response is expected from electronic considerations and, indeed, is observed in $Gd_5Si_{2.75}P_{1.25}$ in the form of $T1-T1$ dimer cleavage. For simplicity, we assume that the transition also occurs in "Gd_5Si_3P." By treating the monomers resulting from the $T1-T1$ dimer cleavage to be isoelectronic with noble gas atoms, "Gd_5Si_3P" can be formulated as $(Gd^{3+})_5(Si_2^{6-})(Si^{4-})(P^{3-})(2e^-)$ when P is on the $T1$ site or $(Gd^{3+})_5([SiP]^{5-})(Si^{4-})_2(2e^-)$ when P is on the $T2$ or $T3$ site. As seen, the interslab dimer cleavage absorbs the extra electrons and preserves the intraslab dimers and integrity of the slabs themselves.

Using chemical considerations, it should also be possible to predict site preference for the P atoms. Three models are considered here: in Model **1**, the 4 P atoms occupy one-half of the $T1$ sites in a way that the nearest P neighbors are only Si1 atoms; in Models **2** and **3**, the P atoms are on the $T2$ and $T3$ sites, respectively. The environments around the $T2$ and $T3$ sites are quite similar, but significantly different from that around the $T1$ site. Thus, it should be possible to differentiate between

(37) Mozharivskyj, Y.; Pecharsky, A. O.; Pecharsky, V. K.; Miller, G. J.; Gschneidner, J.; Karl, A. *Phys. Rev. B* **2004**, *69*, 144102.

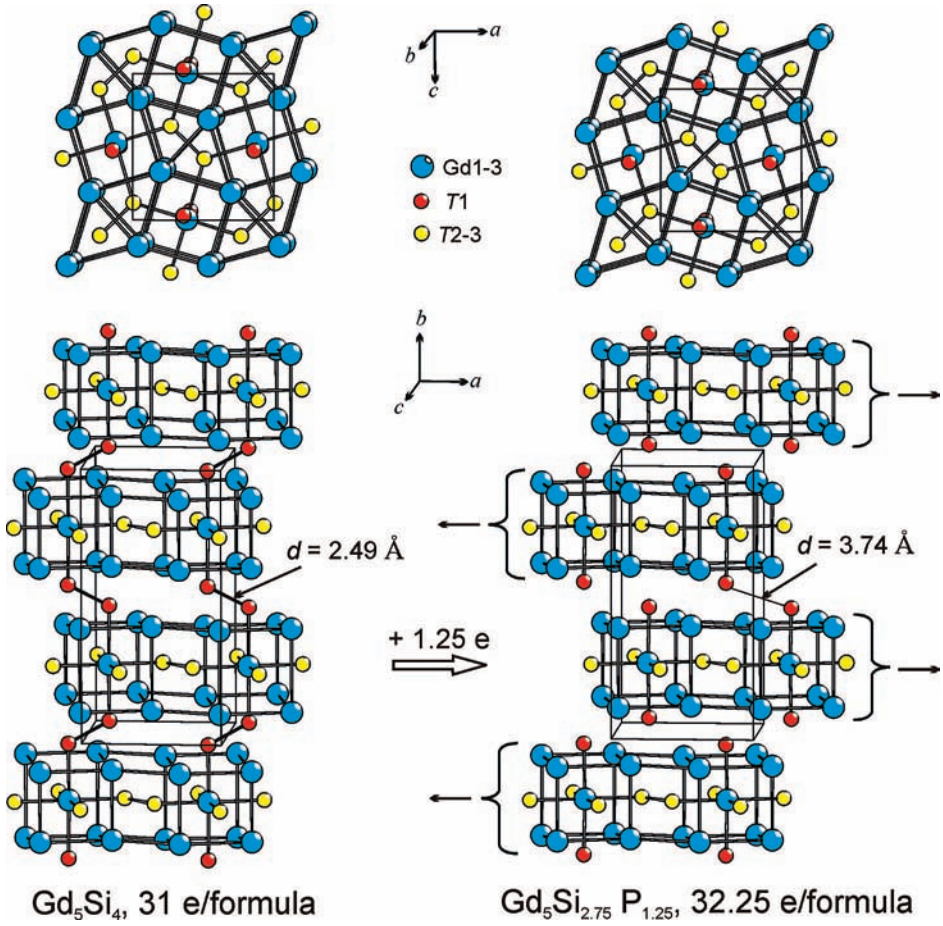

Figure 3. Crystal structure of Gd_5Si_4 and $Gd_5Si_{2.75}P_{1.25}$ as projected along *b* (top) and *c* directions (bottom). Movement of the slabs in $Gd_5Si_{2.75}P_{1.25}$, which leads to the *T*1−*T*1 dimer cleavage, is represented by arrows.

Table 4. Average Interatomic Distances in Gd_5Si_4 and $Gd_5Si_{2.75}P_{1.25}$[a]

bonds	Gd_5Si_4 *d*, Å	$Gd_5Si_{2.75}P_{1.25}$ *d*, Å
Distances within the slabs		
*T*2−*T*3 (×1)	2.484	2.529
Gd−*T*2 (×8)	3.056	3.064
Gd−*T*3 (×8)	3.077	3.063
Gd−Gd (×10)	3.885	3.889
Distances between the slabs		
*T*1−*T*1 (×1)	2.491	3.741
Gd−*T*1 (×16)	3.108	3.082
Gd−Gd (×5)	3.871	4.037

[a] Number of bonds per formula unit is given in parentheses.

the preference of P for the *T*1 site and the *T*2/*T*3 site. Distribution of different atoms over two or more independent sites is known as a coloring problem.[38] While the entropy contribution to the Gibbs free energy always favors statistical distribution of a mixture of elements, electronic and geometric factors usually dictate atomic separation.[39]

In "Gd_5Si_3P" size effects seem to be less important than electronic effects. According to covalent radii (r_{cov}(Si) = 1.17 Å; r_{cov}(P) = 1.10 Å),[20] P atoms should prefer sites with smaller coordination volumes while also leading to smaller unit cell volumes than in Gd_5Si_4. However, unit cell volumes increase with P substitution. With regard to electronic effects, the two itinerant electrons indicated in the formulations of "Gd_5Si_3P" above will partially occupy σ_p* antibonding states within the intraslab *T*2-*T*3 dimers. Because P is more electronegative than Si ($\chi_P = 2.25$ vs $\chi_{Si} = 1.92$),[40] its σ_p* antibonding states within the intraslab dimers would be lower in energy and more populated than those of Si. Thus, having P atoms on the *T*1 site results in a lower electronic energy than placing P atoms on the *T*2 or *T*3 sites. This simple reasoning is supported by the band structure calculations. The TB-LMTO-ASA analysis predicts that the total electronic energy of Model **1** will be 2.56 eV/unit cell lower than that of Model **2** and 3.64 eV/unit cell lower than that of Model **3**. Although there is no experimental proof at this stage to substantiate our conclusions for the site preferences in $Gd_5Si_{4-x}P_x$, the previous studies on the $Gd_5Si_2Ge_2$[41] and $Gd_5Si_{4-x}Sn_x$[18] phases point to a very good agreement between the theoretical findings and experimental data.

Calculated DOS and COHP curves for the Model **1** of "Gd_5Si_3P" are presented in Figures 4 and 5. Presence of the P and Si monomers at the *T*1 sites with very weak *T*1-*T*1 bonding affects both the DOS and COHP curves. The two most prominent features of the DOS of "Gd_5Si_3P," as compared to

(38) Miller, G. J. *Eur. J. Inorg. Chem.* **1998**, *5*, 523–536.
(39) Mozharivskyj, Y.; Franzen, H. F. *J. Alloys Compd.* **2001**, *319*, 100–107.
(40) Mann, J. B.; Meek, T. L.; Allen, L. C. *J. Am. Chem. Soc.* **2000**, *122*, 2780–2783.
(41) Samolyuk, G. D.; Antropov, V. P. *J. Appl. Phys.* **2002**, *91*, 8540–8542.

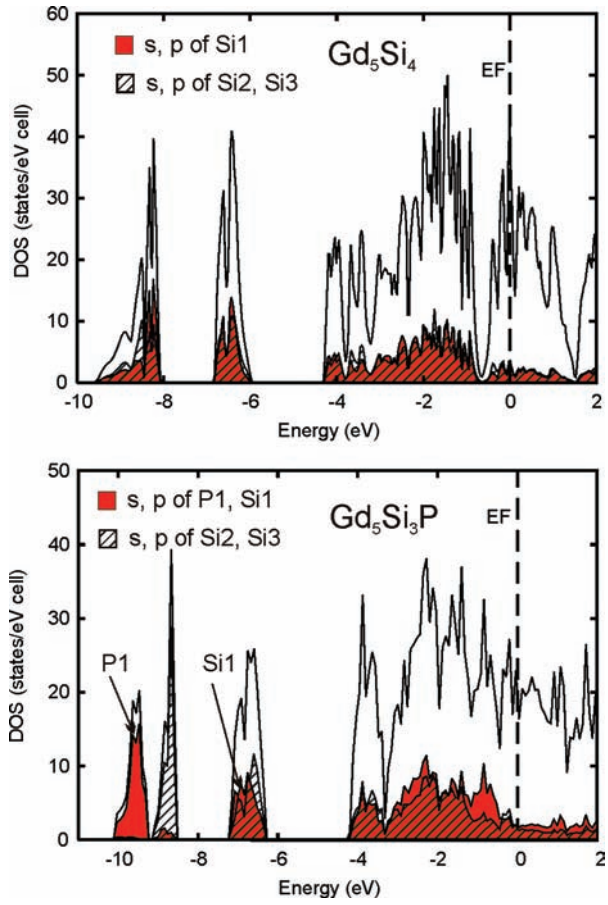

Figure 4. Total and projected densities of states (DOS) for Gd_5Si_4 and "Gd_5Si_3P".

that of Gd_5Si_4, are (i) appearance of an additional DOS peak around −10 eV and (ii) disappearance of the pseudogap. These changes in the DOS are direct consequences of the dimer breaking, with the first feature also reflecting the higher electronegativity of P as compared to Si. The peak around −10 eV originates almost entirely from the nonbonding P1 3*s* orbitals, with its counterpart Si1 nonbonding 3*s* orbitals overlapping the antibonding σ_s* states of the Si2−Si3 dimers. The peak position at −10 eV mirrors the energy of the P1 3*s* orbitals, as the weak interaction between P1 and Si1 is not expected to shift the P1 3*s* states to significantly lower energies. A small energetic dispersion is also expected for the P1 and Si1 3*p* states, which, in turn, leads to a larger DOS at lower energies and, thus, elimination of the pseudogap.

The *T*1−*T*1 dimer cleavage leads to strengthening of the Gd-*T*1 bonds in "Gd_5Si_3P." The COHP calculations show appearance of the additional Gd−*T*1 bonding states around −0.7 eV (Figure 5). Such reinforcement of the Gd−*T*1 interactions is expected from chemical considerations, as the *T*1 electrons freed from the *T*1−*T*1 bonds are donated to the Gd−*T*1 interactions. Integrated COHP (-ICOHP) values calculated for Gd−*T*1 interactions are significantly larger for "Gd_5Si_3P" than for Gd_5Si_4 (13.63 vs 8.99 eV/cell). An increase in Gd−*T*1 bonding correlates well with the changes in Gd−*T*1 interatomic distances (Table 4). During the Gd_5Si_4-to-$Gd_5Si_{2.75}P_{1.25}$ transition, the average Gd−*T*1 bond distance decreases from 3.108 Å in Gd_5Si_4 to 3.082 Å in $Gd_5Si_{2.75}P_{1.25}$. In addition, Gd−Gd interactions become weaker during the transition as represented by the average interslab Gd−Gd distances and calculated -ICOHP values (3.67 vs 4.86 eV/cell for "Gd_5Si_3P" and Gd_5Si_4, respectively). Thus, there is an energetic tradeoff in interactions during the structural transformation: as the interslab *T*1−*T*1 and Gd−Gd interactions became weaker, the Gd−*T*1 bonds became stronger.

The *T*1−*T*1 bonds appear to break up abruptly with an increasing VEC in $Gd_5Si_{4-x}P_x$. Only two atomic arrangements, one with dimers intact ($d_{T1\text{-}T1}$ = 2.49 Å in Gd_5Si_4) and the other with completely broken dimers ($d_{T1\text{-}T1}$ = 3.74 Å in $Gd_5Si_{2.75}P_{1.25}$), are observed in this system. Indirectly, the composite nature of the single crystals from the two-phase region supports this argument. Also, the powder diffraction data (Figure 1) indicate existence only of the Gd_5Si_4- and Sm_5Ge_4-type phases, and no phases with intermediate unit cell parameters and, thus, no intermediate dimer distances were seen, even in the two-phase region. Small variations in the lattice constants for the Sm_5Ge_4-type phases may indicate some variations in the interslab distances, but these variations are expected to be small and the bonds are expected to be fully broken. At present, it is not fully understood why there is a sudden change in the interslab *T*1−*T*1 interactions instead of gradual bond stretching. It can be assumed that a structure with intermediate *T*1−*T*1 distances is unstable with respect to the Gd_5Si_4- and Sm_5Ge_4-type structures. A similar, abrupt dimer cleavage was observed in the $Gd_5Ga_xGe_{4-x}$ system, where introducing an extra 0.3 electron into Gd_5GaGe_3 ($d_{T1\text{-}T1}$ = 2.93 Å) leads to complete dimer cleavage in $Gd_5Ga_{0.7}Ge_{3.3}$ ($d_{T1\text{-}T1}$ = 3.46 Å) and to a first-order phase transition.[17] Analysis of the lattice constants of the $Gd_5Si_xGe_{4-x}$ compounds also points to an abrupt dimer cleavage as a function of Si content,[42] which supports the argument that in some systems stabilization of intermediate structures may not be possible.

Structure vs Electron Count in RE_5T_4 Phases. The current work on the $Gd_5Si_{4-x}P_x$ system clearly demonstrates that the bonding within the interslab *T*-*T* dimers can be disrupted through an increase in the VEC. As discussed above, the atomic sizes are not as influential as electronic factors, i.e., energy band filling and electronegativity, toward controlling these dimer interactions. In fact, if the electronic effects would be neglected, a somewhat smaller size of P would lead to shorter *T*−*T* distances. Additionally, $Gd_5Si_{2.75}P_{1.25}$ extends the existence of RE_5T_4 phases (*RE* is a rare-earth metal, *T* is a *p*-element) with a Sm_5Ge_4-type structure to the VEC of 32.5 e^-/formula unit, above 31 e^- as previously observed.

The electron-richer $RE_5T_2Sb_2$ phases (*RE* = Y, Tb, Dy, Ho, Er, *T* = Si, Ge) have been also reported, but they adopt a different orthorhombic structure (space group *Cmca*), which is an ordered version of the Eu_5As_4 structure.[43] While being similar to the Sm_5Ge_4 structure such that there are no interslab dimers, this new orthorhombic structure has not exhibited any phase transition to reform dimers, and the absence of *T*/Sb mixing in their atomic arrangements suggests a simple structural adaptation for the larger Sb atoms. In $RE_5T_2Sb_2$, the Sb atoms are located between the slabs, while *T* atoms form dimers within the slabs. As discussed for "Gd_5Si_3P," the more electronegative atoms prefer to occupy sites with no homonuclear bonds in order to minimize the total electronic energy. If the two sites in $RE_5T_2Sb_2$ could be occupied by both Si and Sb, then Si would be expected to fill in the interslab sites and Sb to form intraslab dimers.

(42) Pecharsky, A. O.; Gschneidner, K. A., Jr.; Pecharsky, V. K.; Schindler, C. E. *J. Alloys Compd.* **2002**, *338*, 126–135.
(43) Kozlov, A. Y.; Pavlyuk, V. V.; Davydov, V. M. *Intermetallics* **2004**, *12*, 151–155.

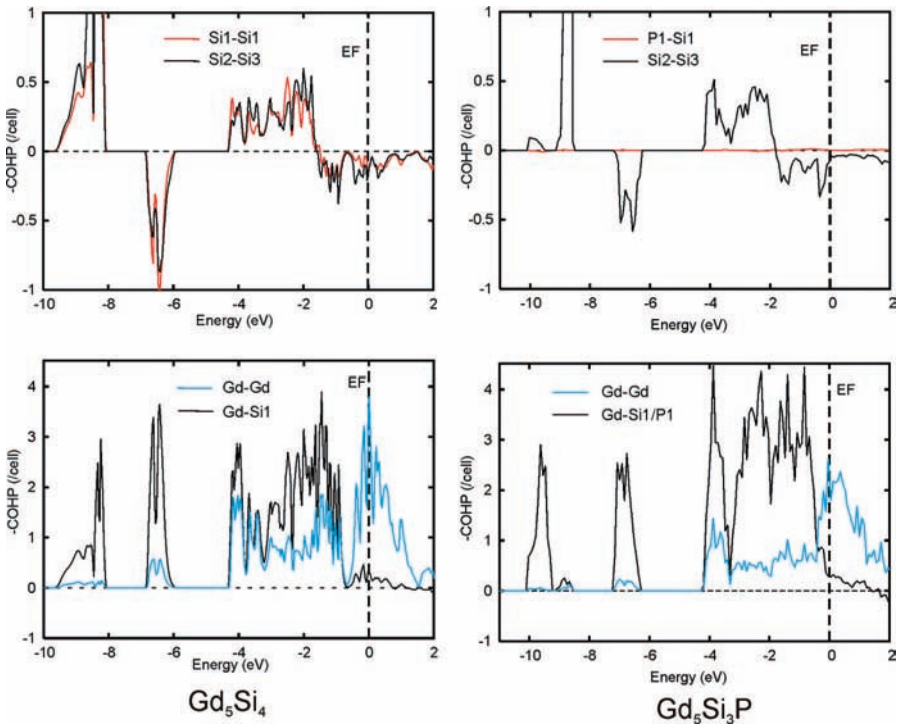

Figure 5. Crystal orbital Hamilton population (COHP) curves for some interactions in Gd_5Si_4 and "Gd_5Si_3P". Interactions in the upper part are bonding and in the lower part are antibonding.

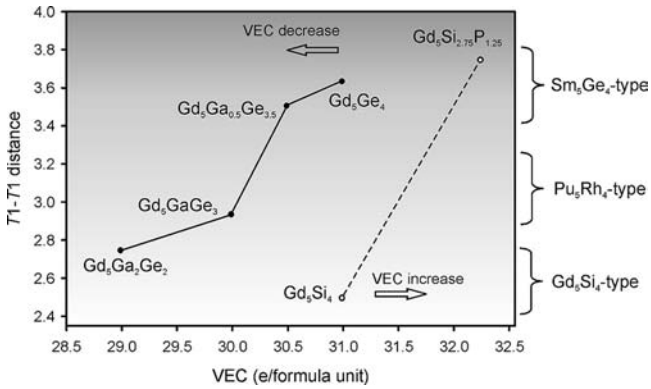

Figure 6. Interslab dimer distances in the $Gd_5Ga_xGe_{4-x}$ and $Gd_5Si_{4-x}P_x$ phases as a function of valence electron concentration. Only single crystal data from single-phase samples are used. Data for $Gd_5Ga_xGe_{4-x}$ are taken from ref 17. The existence ranges for the three structure types are shown.

Therefore, the $RE_5T_2Sb_2$ structures adapt to the larger Sb atoms rather than respond to the increased VEC. This type of structural adaptation was also observed in $Gd_5Si_{4-x}Sn_x$, where substitution of Si with electron-equivalent, but larger, Sn led to dimer cleavage.[18] There are two contradictory reports regarding the existence of $Gd_5Si_2Sb_2$, with one claiming that the phase cannot be obtained[43] and the other one stating that $Gd_5Si_2Sb_2$ adopts a Sm_5Ge_4-type structure as observed from X-ray powder diffraction (however, the diffraction profile was not provided).[44] We will refrain from discussing $Gd_5Si_2Sb_2$ until further studies are done.

The current study on the $Gd_5Si_{4-x}P_x$ system complements the previous studies on the $Gd_5Ga_xGe_{4-x}$ system. In $Gd_5Ga_xGe_{4-x}$, the lower VEC led to reforming the interslab $T1-T1$ dimers by substituting Ga for Ge in the 31 e^- Gd_5Ge_4 phase, which adopts the Sm_5Ge_4-type structure. On the other hand, in $Gd_5Si_{4-x}P_x$, the higher VEC manifested breaking the interslab $T1-T1$ dimers in the 31 e^- Gd_5Si_4 phase by replacing Si with P atoms. Figure 6 shows the dependence of the interslab $T1-T1$ dimer distances as a function of VEC for various Gd_5T_4 single crystals. While being similar in its nature, the two approaches differ with respect to the targeted phases and potential outcome. In particular, in a structure with the interslab dimers intact, an increase in the VEC is expected to break the dimers. Obviously, doing so in a phase with already broken dimers will have no structural consequences, and, thus, the opposite direction, namely reduction in the VEC, has to be pursued. We believe that the two approaches can be extended to other RE_5T_4 phases and may be utilized in predicting and, subsequently, obtaining new phases.

Conclusions

Structural transformations in the $Gd_5Si_{4-x}P_x$ system prove that a higher VEC can be used to break interslab $T-T$ dimers in Gd_5Si_4-type phases and, thus, to induce a Gd_5Si_4-to-Sm_5Ge_4 phase change. Also, the existence of the Sm_5Ge_4-type phases is extended to VEC values larger than 31 e^-/formula unit. The driving force for the phase transition in $Gd_5Si_{4-x}P_x$ and RE_5T_4 phases, in general, is optimization of interslab $T-T$ bonding, which leads to $T-T$ dimer cleavage at higher VEC values and their recombination at lower VEC values.

Acknowledgment. This work was supported by a Discovery Grant from the Natural Sciences and Engineering Research Council of Canada.

Supporting Information Available: Supplementary crystallographic data (cif). This material is available free of charge via the Internet at http://pubs.acs.org.

JA8085033

(44) Nirmala, R.; Morozkin, A. V.; Malik, S. K. *Europhys. Lett.* **2005**, *72*, 652–657.